Nano Research

Open Access

Review Article

NO-to-NH_3 conversion under real flue-gas conditions: Environmental catalysis and challenges toward sustainable deployment

Ye He[1], Haoqing Ji[1], Jianping Sheng[1]✉, Fan Dong[2], and Yanjuan Sun[1]✉

[1] School of Resources and Environment, University of Electronic Science and Technology of China, Chengdu 611731, China
[2] Research Center for Carbon-Neutral Environmental & Energy Technology, Institute of Fundamental and Frontier Sciences, University of Electronic Science and Technology of China, Chengdu 611731, China

Cite this article: *Nano Research*, **2026**, *19*, 94908489. https://doi.org/10.26599/NR.2026.94908489

ABSTRACT: The catalytic reduction of nitric oxide (NO) to ammonia (NO reduction reaction (NORR)) provides a dual-benefit environmental pathway that simultaneously mitigates harmful NO emissions and supports sustainable nitrogen management. Significant advances have been made in understanding active-site structures, orbital hybridization, and proton-coupled electron-transfer steps governing NO activation and selectivity. However, most progress has been achieved under idealized laboratory conditions, whereas real flue-gas environments pose substantial challenges to catalyst stability, competitive adsorption, reaction pathways, and system integration. This review critically evaluates mechanistic insights, catalyst design principles, and emerging reactor configurations relevant to NORR under practical conditions. By integrating environmental catalysis with process engineering considerations, we outline strategies to enhance selectivity, impurity tolerance, and operational robustness. Finally, key research priorities and sustainability implications are identified to guide the advancement and deployment of NORR technologies for resource-oriented utilization of industrial flue gas NO streams.

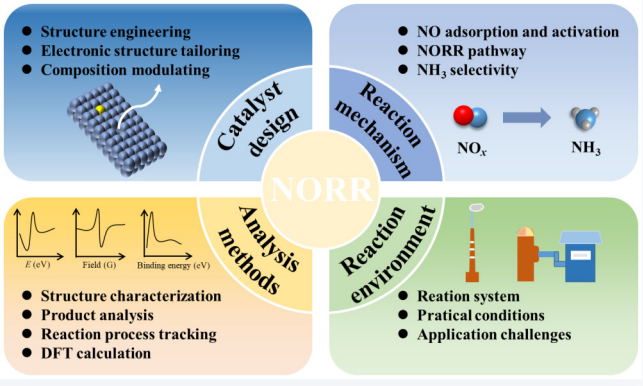

KEYWORDS: nitric oxide, nitric oxide reduction reaction, NO reduction, NH_3 synthesis, mechanism

1 Introduction

Nitric oxide (NO) is the major air pollutant produced by fossil fuel combustion and vehicle exhaust emissions [1–3]. Direct NO emissions contribute to acid rain, photochemical smog, and particulate matter formation, thereby posing serious risks to human health and exerting adverse impacts on socioeconomic activities [4, 5]. In recent years, selective catalytic reduction (SCR), converting NO into N_2 with NH_3, has become the most widely applied and effective industrial technology for NO abatement [6–10]. However, SCR requires high operating temperatures (300–400 °C), resulting in energy consumption and operational costs [10–12]. Furthermore, from the perspective of nitrogen utilization, SCR requires an external supply of ammonia and does not directly utilize the nitrogen contained in NO. These limitations underscore the need for innovative and practical catalytic strategies that enable both efficient NO removal and high-value utilization of nitrogen-containing compounds [13, 14].

Ammonia plays a crucial role in the natural nitrogen cycle and human society [15–19]. As a hydrogen carrier, ammonia represents a resource of considerable value. At present, industrial ammonia production is dominated by the Haber–Bosch process, which employs N_2 and H_2 as feedstocks operating under high temperature (300–500 °C) and high pressure (15,000–30,000 kPa) [20–22]. The Haber–Bosch process consumes nearly 2% of the total global energy supply [23, 24]. Consequently, the development of energy-efficient and sustainable alternatives for ammonia synthesis is important. Recent studies have explored photo/electrocatalytic nitrogen reduction reaction (NRR) under ambient conditions as a promising green strategy for ammonia production [16, 25–28]. Meanwhile, NRR has achieved preliminary success at the laboratory

Received: December 25, 2025; **Revised:** January 6, 2026
Accepted: January 25, 2026

✉Address correspondence to Jianping Sheng, jpshengchn@163.com; Yanjuan Sun, sunyj@uestc.edu.cn

scale. However, the strong N≡N bond (941 kJ·mol^{-1}) limits reaction kinetics, resulting in low NH_3 yields and conversion efficiencies. In comparison, NO reduction reaction (NORR) requires overcoming the N=O bond energy (631 kJ·mol^{-1}), which reduces the energy barrier. Ammonia synthesis via NORR under mild conditions simultaneously enables pollutant removal and nitrogen resource recovery from industrial flue gas [29–37]. With continued advances in catalyst design and process optimization, the NH_3 selectivity and yield of NORR have improved in recent years, providing a foundation for prospective industrial applications. Within the broader context of green chemistry and sustainable development, NORR exhibits potential as a key direction for the future development of ammonia synthesis.

Although extensive efforts have been devoted to the development of catalytic systems for NO-to-NH_3 conversion, most studies have been carried out under idealized laboratory conditions with purified reactants and simplified reaction environments [30, 38–41]. Typical industrial flue gas contains NO at concentrations of 100–1000 ppm, together with O_2 (3 vol.%–10 vol.%), CO_2 (5 vol.%–15 vol.%), H_2O vapor, and trace impurities, such as SO_2 and particulates. The realistic coexisting components can significantly alter reaction thermodynamics, intermediate stability, and catalyst durability, which remain insufficiently understood. In contrast, many laboratory studies employ purified NO feeds at concentrations above 1 vol.% under simplified atmospheres, which may overestimate intrinsic activity and selectivity. To achieve practical applicability, future research should therefore move beyond ideal systems and explore the catalytic behavior under realistic operating conditions.

This review provides a comprehensive overview of recent advances in ammonia synthesis from NO reduction (Fig. 1), focusing on high-performance catalyst design, mechanistic understanding of NORR pathways, insights derived from *in situ* characterizations, and the adaptability of reaction systems under conditions relevant to practical applications. By summarizing current achievements, identifying knowledge gaps, and outlining future perspectives, we aim to highlight key scientific and technological directions required to bridge the gap between fundamental studies and practical applications.

2 Catalyst design strategies

The efficiency of the NORR is governed by the ability of catalysts to regulate the adsorption, activation, and transformation of reaction intermediates while suppressing competing pathways. These processes are intrinsically linked to the structural, electronic, and compositional characteristics of catalytically active sites. In this section, recent progress in structure engineering, electronic structure tailoring, and compositional modulation is briefly summarized to highlight general design strategies relevant to selective ammonia synthesis.

2.1 Structure engineering

Structural engineering provides a fundamental approach to tuning NORR performance by regulating crystal phase, exposed facets, and atomic arrangements, which collectively define the coordination environment and electronic states of active sites. These structural features influence adsorption strength, activation barriers, and migration kinetics of key intermediates, thereby governing catalytic activity and product selectivity [42, 43].

Phase engineering tailors the bulk electronic configuration. For instance, hexagonal-close-packed cobalt (hcp-Co) nanosheets, compared to their face-centered cubic (fcc-Co) counterparts, exhibit enriched spin-polarized electrons near the Fermi level (Figs. 2(a)–2(c)), which facilitates proton transfer and leads to a substantial enhancement in NH_3 yield under pure NO gas [44]. Facet engineering provides atomic-level control over surface reactivity by designing specific arrangements of undercoordinated sites. High-index Ni (210) facets with a high density of step sites can optimize intermediate binding configurations and lower migration barriers, resulting in Faradaic efficiencies (FE) for NH_3 approaching 100% (Fig. 2(d)) [45].

Overall, these studies demonstrate that rational structural control offers an effective means to tune adsorption behavior and reaction pathways, providing a structural basis for improving NORR activity and selectivity.

2.2 Electronic structure tailoring

Beyond geometric considerations, electronic structure tailoring enables direct optimization of charge distribution, d-band states, and local coordination, without altering the underlying crystal

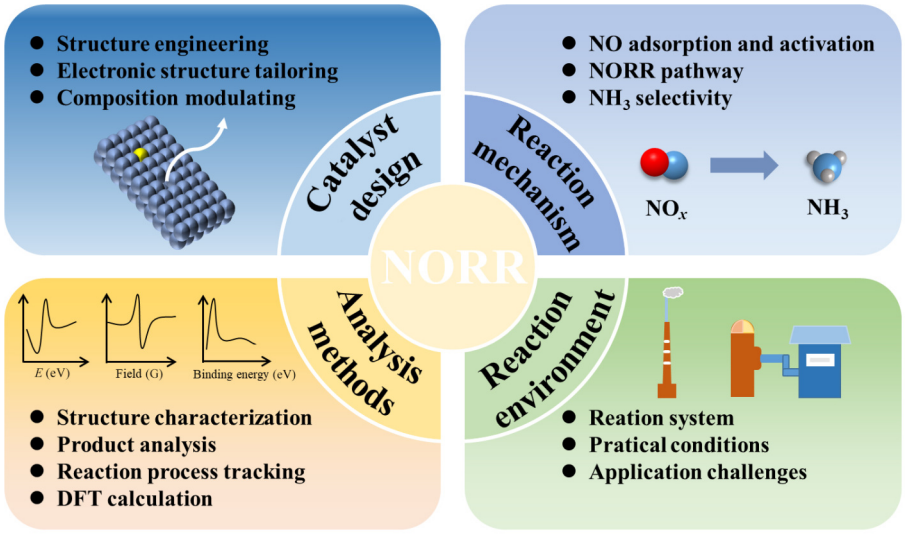

Figure 1 Schematic illustration of recent advances in NORR for ammonia synthesis.

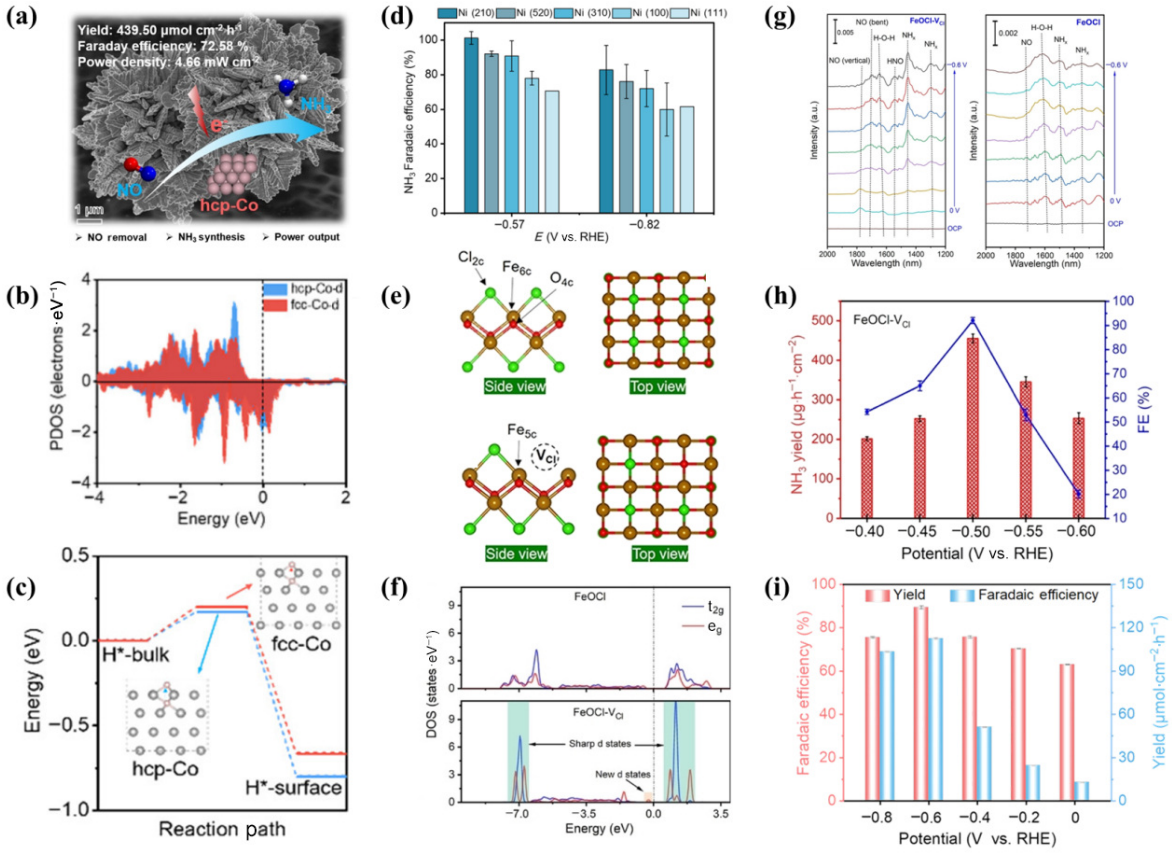

Figure 2 (a) Morphology and structure of hcp-Co. (b) Projected density of states (PDOS) of the d-orbitals in hcp-Co and fcc-Co. (c) Diffusion processes of protons from the bulk to the surface of two catalysts. ((a)–(c)) Reproduced with permission from Ref. [44], © American Chemical Society 2023. (d) Faradaic efficiency of NH_3 on five single-crystal Ni foils with different facets. Reproduced with permission from Ref. [45], © Elsevier Inc. 2023. (e) Atom configurations of pristine FeOCl and FeOCl-VCl. (f) DOS of Fe in FeOCl and FeOC-VCl. (g) *In situ* attenuated total reflection IR (ATR-IR) spectra of FeOCl-VCl and FeOCl for NORR at different potentials. (h) NH_3 yield and FE of FeOCl-VCl with 1 vol.% NO feed. ((e)–(h)) Reproduced with permission from Ref. [51], © Wiley-VCH GmbH 2023. (i) NH_3 yield and FE of CuFe DS/NC at various potentials. Reproduced with permission from Ref. [59], © Wiley-VCH GmbH 2023.

structure. Defect engineering, including the introduction of vacancies or lattice distortions, is a widely employed strategy to generate localized electronic states that stabilize key intermediates and facilitate charge transfer [46–50]. For instance, Guo et al. introduced chlorine vacancies in FeOCl nanosheets (Fig. 2(e)), which lowered the average oxidation state of Fe and generated sharp d-states [51]. These electronic modifications strengthened the electronic coupling with NO intermediates (Fig. 2(f)), facilitating the formation of key NHO and NH_x species (Fig. 2(g)), enabling an NH_3 yield of 455.4 μg·cm^{-2}·h^{-1} under 1 vol.% NO concentration (Fig. 2(h)). Such results underscore that localized electronic modulation provides a complementary strategy to structure engineering, thereby offering distinct advantages for NO-to-NH_3 conversion.

2.3 Composition modulating

Composition modulation provides an additional degree of freedom in catalyst design by tailoring the chemical identity and interactions of active centers. Atomic-scale integration of multiple elements creates new coordination environments and synergistic effects that regulate adsorption behavior, electronic structure, and reaction pathways, enabling catalytic functionalities beyond those of single-component systems [52].

The construction of atomic-scale active sites is a prime example. While single-atom catalysts (SACs) maximize atom utilization and can effectively activate NO [53–55], their isolated nature often limits electronic coupling and complex reaction dynamics. Peng et al. synthesized Nb, Al, Mn, Fe, and Cu SACs supported on B, N co-doped carbon nanotubes, which achieved Faradaic efficiencies below 78%, indicating room for improvement [56]. To overcome these limitations, dual-atom catalysts (DACs) exploit metal–metal synergy to enable interatomic electron delocalization and cooperative adsorption, thereby modulating the electronic structure and reaction pathways [57, 58]. Wang et al. developed an atomic Cu–Fe dual-site (DS) catalyst (CuFe DS/nitrogen-doped carbon (NC)), achieving a Faradaic efficiency of 90% for NH_3 yield of 112.52 μmol·cm^{-2}·h^{-1} (Fig. 2(i)), surpassing its single-atom counterparts [59]. The Cu–Fe pair facilitates interatomic electron delocalization, which weakens NO adsorption and favorably shifts the rate-determining step, thereby accelerating the overall hydrogenation kinetics.

Collectively, composition modulation through atomic-scale alloying or multi-metal synergy provides a powerful route to fine-tune adsorption strength, charge transfer, and reaction pathways. However, it should be noted that although these structure-engineered catalysts were evaluated under ideal NO feeds, their performance and durability under O_2/SO_2-containing real flue-gas remain insufficiently explored. Future studies should integrate structure control with environmental-resilience requirements.

3 Reaction pathways and mechanisms

Nitric oxide possesses an unpaired electron in its antibonding π* orbital, rendering the N–O bond readily activatable [60–63]. Nevertheless, NORR involves complex proton-coupled electron transfer (PCET) processes, oxygen removal steps, and competition between ammonia formation and side reactions. Understanding how NO adsorbs, activates, and transforms on catalyst surfaces is therefore essential for rational catalyst design.

3.1 NO adsorption and activation

The initial adsorption and activation of NO on catalyst surfaces are critical steps that largely determine the overall efficiency of NORR. The process is governed by the "donation–backdonation" mechanism, a fundamental orbital interaction wherein the transition metal center accepts electron density from the lone pair of NO into its empty d-orbitals, while simultaneously back-donating electrons from its filled d-orbitals into the antibonding π* orbital of NO (Fig. 3(a)). This synergistic electron transfer achieves dual effects: It strengthens the metal–NO bond for effective adsorption, and populates the NO π* orbital, thereby weakening the N–O bond and priming it for subsequent reduction.

The efficacy of this mechanism is evidenced across diverse catalysts. On Cu (111) surfaces, a σ–π hybridization variant of this mechanism facilitates robust adsorption, contributing to a record NO conversion efficiency exceeding 63.74% under electrochemical conditions (Fig. 3(b)) [62]. Similarly, in hcp-Co nanosheets, spin-polarized electrons from Co d-orbitals near the Fermi level directly back-donate into the NO π* orbital, forming a d–π* bond (Fig. 2(b)) [44]. This specific interaction elongates the N–O bond from 1.169 to 1.228 Å, significantly enhancing activation and subsequent protonation kinetics.

Overall, orbital hybridization induces electron transfer that selectively weakens the N–O bond, promoting NO adsorption and activation and facilitating subsequent protonation for ammonia formation. This electronic interaction is particularly critical under real flue-gas conditions where NO typically exists at low concentrations and competes with O_2 and H_2O for adsorption sites.

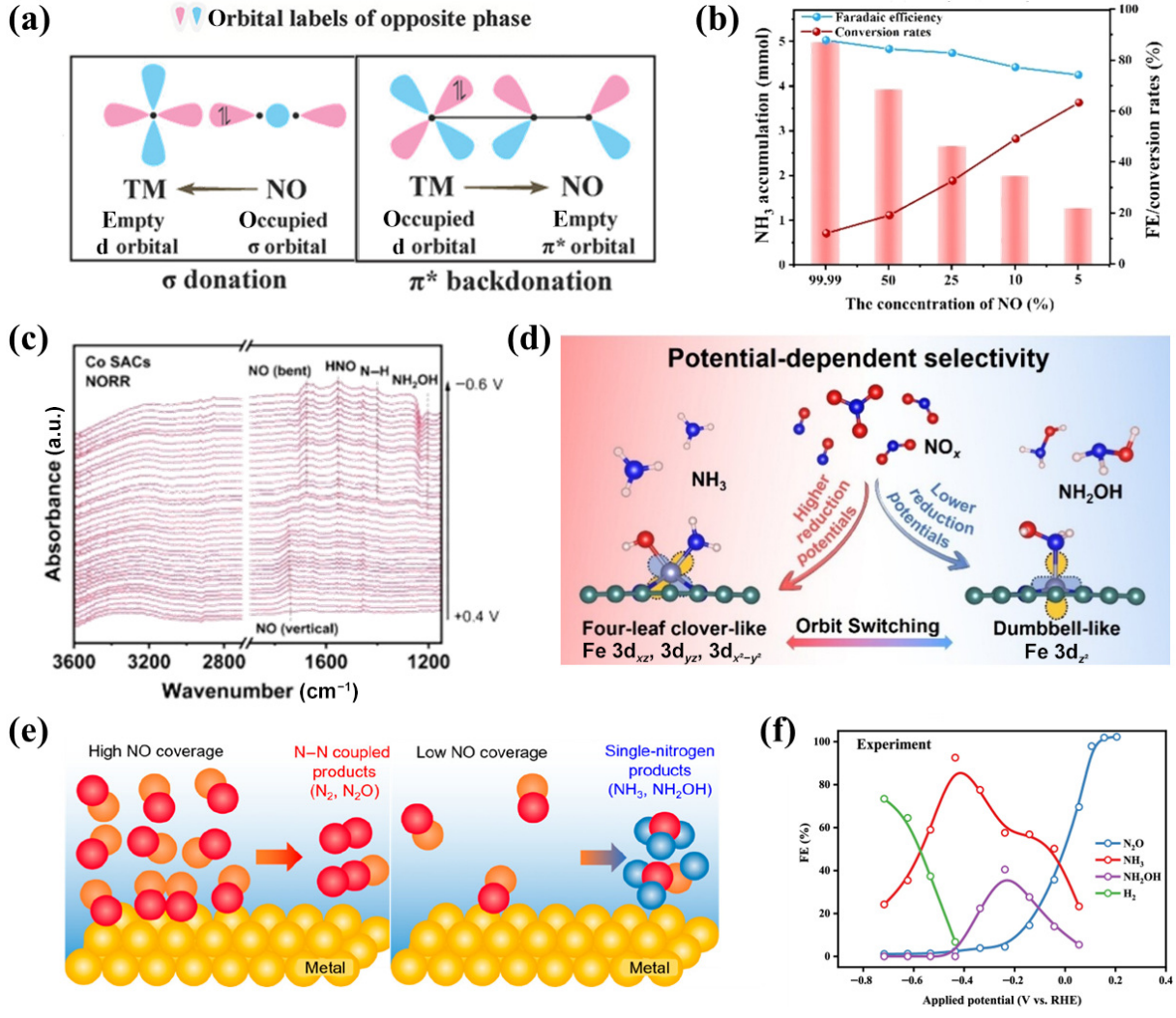

Figure 3 (a) Schematic of the interaction between transition metals and NO. Reproduced with permission from Ref. [106], © Wiley-VCH GmbH 2021. (b) NO conversion ratio and Faradaic efficiency of NORR under different NO concentrations. Reproduced with permission from Ref. [62], © Wiley-VCH GmbH 2024. (c) Potential-dependent *in situ* ATR-IR spectra of NORR on Co SACs. Reproduced with permission from Ref. [72], © Wiley-VCH GmbH 2023. (d) Schematic of potential-induced Fe orbital switching regulating product selectivity in NORR. Reproduced with permission from Ref. [73], © American Chemical Society 2025. (e) Schematic of product selectivity under high NO coverage and low NO coverage. Reproduced with permission from Ref. [75], © American Chemical Society 2022. (f) Experimental Faradaic efficiencies of NORR products on Ag. Reproduced with permission from Ref. [76], © American Chemical Society 2021.

By enhancing the intrinsic affinity and activation capability toward dilute NO, orbital-hybridization-driven pathways provide actionable guidance for designing catalysts capable of operating in compositionally complex industrial gas streams.

3.2 NORR pathway

NORR can proceed via dissociative or associative pathways, depending on whether N–O bond cleavage occurs prior to hydrogenation or through stepwise protonation of NO-derived intermediates [40]. In the dissociative pathway, the N–O bond is cleaved prior to significant hydrogenation, yielding adsorbed N* and O* atoms that are subsequently protonated to NH_3 and H_2O. Conversely, the associative pathway involves the sequential hydrogenation of the intact NO molecule or its partially hydrogenated derivatives (e.g., H_xNOH_y), with N–O bond scission occurring at a later stage.

These pathways differ in the sequence of PCET steps and the nature of key intermediates, leading to distinct kinetic barriers and product selectivity. In general, pathway preference is governed by the relative stability of hydrogenated intermediates and the associated reaction energy barriers, which collectively determine catalyst-dependent selectivity trends and also influence which elementary step becomes rate-limiting under realistic reaction conditions, while structural features favoring high activity may also pose challenges for long-term stability.

In summary, NORR is a multi-step process involving multiple pathways, including N–O bond cleavage, proton–electron transfer, and intermediate transformations. Detailed understanding of these pathways and intermediates provides a mechanistic foundation for further studies on catalyst performance and reaction control.

3.3 NH_3 selectivity

Achieving high selectivity for NH_3 in NORR requires steering the reaction away from a complex network of possible byproducts, including N_2, N_2O, and NH_2OH, and H_2 (from the competing hydrogen evolution reaction (HER)) [64–71]. Here, NH_3 selectivity refers to different performance metrics depending on the reaction system, such as Faradaic efficiency in electrocatalytic studies or product selectivity and conversion efficiency in thermocatalytic and photocatalytic systems. Selectivity is governed by the interplay of intrinsic catalyst properties and extrinsic reaction conditions, which collectively determine the stability of key intermediates and the relative rates of competing pathways.

Intrinsic factors primarily arise from the atomic and electronic structure of the catalyst. Geometric factors, such as the spatial arrangement of surface atoms, can strongly affect NO adsorption configurations and influence N–O bond activation. For instance, on Co SACs, NO adsorbs linearly on isolated Co sites, maintaining the N–O bond stability [72]. Under these conditions, the reaction predominantly proceeds through HNO and H_2NO intermediates, followed by sequential hydrogenation to NH_2OH, achieving a Faradaic efficiency of 81.3%. In contrast, on Co nanoparticles (Co NPs), NO adopts a bridging adsorption mode. The cooperative interaction between adjacent Co atoms weakens the N–O bond and favors a dissociation pathway that predominantly yields NH_3, with a Faradaic efficiency of 92.3% (Fig. 3(c)).

In addition to geometric factors, the local electronic structure also plays a critical role in modulating reaction pathways. In pyridinic FeN_4, at relatively high reduction potentials (−1.2 to −0.6 V vs. standard hydrogen electrode (SHE)), bidirectional interaction between the cloverleaf-shaped Fe $3d_{xz}$ ($3d_{yz}$ and $3d_{x^2-y^2}$) orbitals and the N/O $2p_z$ orbitals facilitates N–O bond cleavage and strengthens the adsorption of $*NH_2$ and *OH species, thereby favoring NH_3 formation [73]. At lower reduction potentials (−0.6 to 0.6 V vs. SHE), unidirectional interaction with dumbbell-shaped Fe $3d_{z^2}$ orbital is less favorable for N–O bond cleavage, leading to stabilization of the $*NH_2OH$ intermediate and favoring NH_2OH production (Fig. 3(d)). These observations demonstrate that both the atomic arrangement and electronic structure of the catalyst surface are intrinsic factors that critically determine the formation and stability of reaction intermediates in NORR.

External factors, such as NO coverage, electrolyte environment, and applied electrode potential, could also affect product selectivity. NO coverage, influenced by initial NO concentration, dictates the balance between N–N coupling and hydrogenation pathways [74]. High NO coverage promotes coupling among adsorbed species, favoring the formation of N_2O and N_2, whereas low coverage favors single-nitrogen products, such as NH_3 and NH_2OH (Fig. 3(e)) [75]. Critically, this has direct implications for processing real industrial flue gas, where NO concentrations are typically dilute (500–1000 ppm). Therefore, under realistic flue-gas conditions, selectivity control should be discussed in the context of intrinsically low NO surface coverage.

Applied electrode potential alters the energetics of protonation steps. On Ag catalysts, microkinetic simulations and experiments show that increasing the potential to 0.25–0.4 V vs. reversible hydrogen electrode (RHE) lowers the energy barrier for $ONNOH^* \rightarrow N_2O^* + H_2O$, promoting the formation of N_2O [76]. When the potential decreases below 0.25 V vs. RHE, the barrier for the rate-determining step (RDS, $HNOH^* \rightarrow NH^* + H_2O$) is reduced, favoring NH_3 formation. At potentials below −0.65 V vs. RHE, the HER becomes dominant, suppressing NH_3 production and shifting selectivity toward H_2 (Fig. 3(f)), defining a narrow operating window for selective ammonia synthesis. Electrolyte composition and pH further modulate proton availability and adsorption energetics, providing additional handles to tune product distribution [64, 77, 78].

In summary, NORR selectivity arises from the combined effects of intrinsic catalyst properties and external reaction conditions. Understanding how these factors influence the stability of key intermediates and the energetics of hydrogenation pathways provides a mechanistic basis for the rational design of catalysts and optimization of operating conditions to favor selective NH_3 synthesis.

3.4 Probing reaction pathways and mechanisms

Unraveling the reaction pathways of NORR requires direct identification of surface intermediates and tracking the dynamic evolution of active sites under operating conditions. Given the transient nature of reaction intermediates and the complexity of catalytic cycles, *in situ*/*operando* spectroscopies are indispensable for correlating the local coordination/electronic structure with adsorption configurations and product formation. When combined with theoretical calculations, these approaches enable a comprehensive understanding of structure–activity–selectivity relationships, providing a mechanistic basis for rational catalyst and system design.

3.4.1 In situ/operando experimental techniques

A range of *in situ* and *operando* techniques has been developed to

probe NORR, establishing a comprehensive framework linking catalyst structure, reaction, and products (Fig. 4). At the level of catalyst structure and active sites, *in situ* X-ray absorption spectroscopy (XAS) provides atomic-scale information on local coordination environments, valence states, and bond-length evolution, thereby revealing the structural dynamics of active sites under realistic reaction conditions [79]. For example, potential-dependent Fe K-edge X-ray absorption near edge structure (XANES) indicates the reduction of Fe^{3+}-N_xC_y to Fe^{2+}-N_xC_y, suggesting Fe^{2+}-N_xC_y as the catalytically relevant state during NORR (Fig. 5(a)) [66]. *In situ* X-ray photoelectron spectroscopy (XPS) complements XAS by real-time monitoring surface valence-state variations and electronic-structure modulation [80]. For instance, quasi-*in situ* XPS was employed to track light-excited defect formation in photoexcited oxygen vacancies (PV_O)-TiO_2, revealing how these defect sites influence the surface electronic structure (Fig. 5(b)) [81].

For product analysis, online differential electrochemical mass spectrometry (DEMS) enables real-time detection of gaseous intermediates and products, such as NH_3, N_2O, N_2, and other intermediates (Fig. 5(c)) [32]. Nuclear magnetic resonance (NMR), particularly when coupled with ^{15}N isotopic labeling, provides rigorous validation of nitrogen sources and quantification of liquid-phase nitrogen-containing products, excluding external contamination (Fig. 5(d)) [82].

To directly track the surface reaction process, electron paramagnetic resonance (EPR) spectroscopy, sensitive to unpaired electrons, identifies radical species formed during the reaction and provides insights into electron-transfer and hydrogenation processes. *Operando* EPR allows real-time tracking of active-site dynamics, visualizing electron transfer between catalysts and reactants in NORR [83]. Sheng et al. applied *operando* EPR to monitor gas–solid photocatalytic NORR, detecting NO radicals and their interactions with H_2O without the use of trapping agents (Fig. 5(e)) [81]. Complementarily, *in situ* infrared (IR) spectroscopy monitors vibrational signatures of adsorbed NO and hydrogenated intermediates, enabling real-time identification of key surface species (Figs. 5(f) and 5(g)) [62, 84].

Collectively, these complementary techniques, spanning structural dynamics, surface chemistry, intermediate identification, and nitrogen-source tracing, provide a systematic framework for mechanistic elucidation of NORR and support the rational design of catalysts. Based on the research practice of our group, several additional *in situ* characterizations are theoretically applicable to NORR. For instance, *in situ* Raman spectroscopy, which is insensitive to aqueous environments, can probe the structural stability and surface-adsorbed intermediates under realistic water-vapor reaction conditions, complementing *in situ* infrared spectroscopy. In addition, *in situ* photoluminescence (PL), time-resolved PL (TRPL), and *in situ* ultraviolet–visible (UV–Vis) spectroscopy could be applied in NORR to study carrier dynamics and short-lived intermediates. The development of multi-technique *operando* approaches, such as Raman-electrochemistry coupling or EPR-spectroscopy integration, offers a promising route to enhance the understanding of structure–performance–kinetics relationships in NORR.

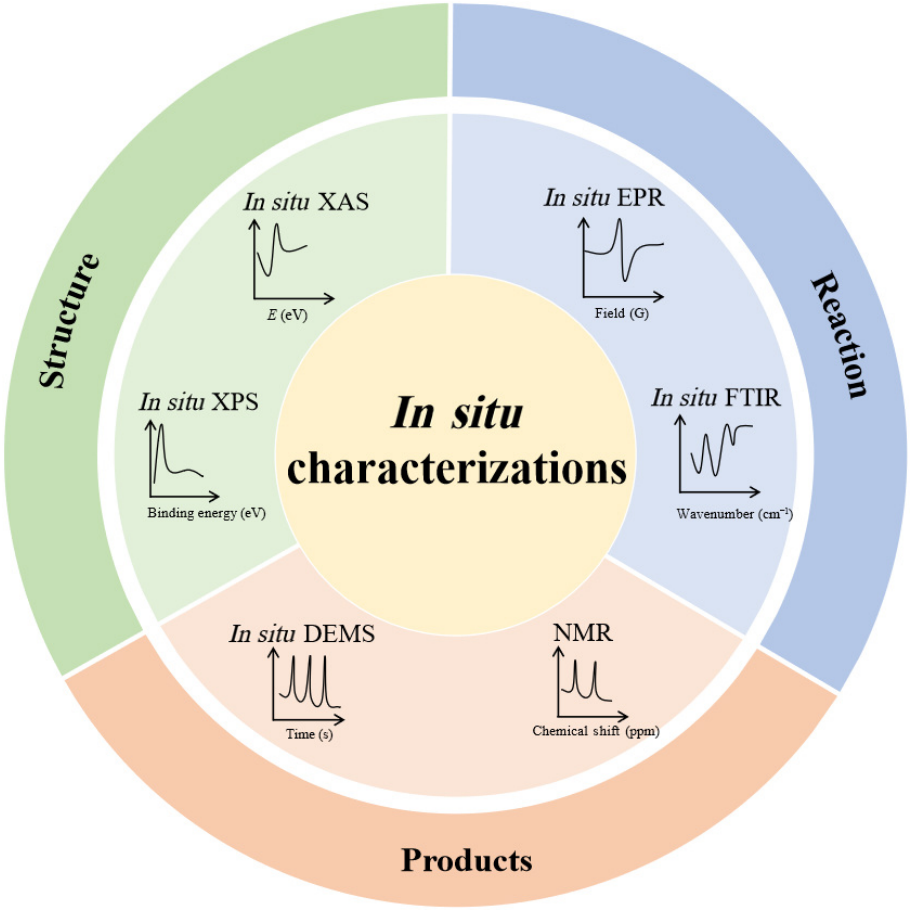

Figure 4 Schematic framework of *in situ* characterization techniques.

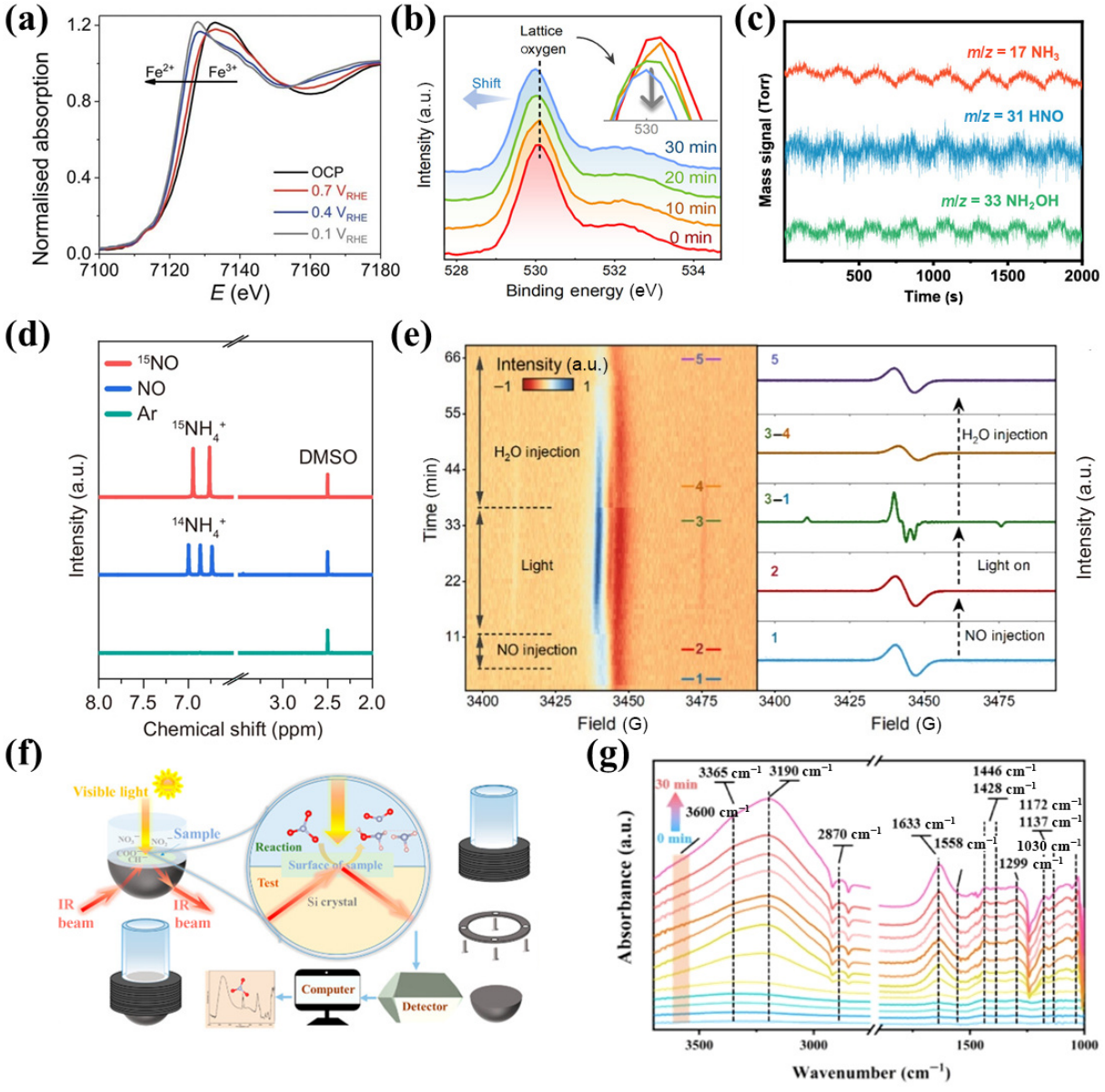

Figure 5 (a) *In situ* XANES spectra of FeNC-dry-0.5 at different potentials. Reproduced with permission from Ref. [66], © Kim, D. H. et al. 2021. (b) Quasi-*in situ* XPS spectra under light irradiation. Reproduced with permission from Ref. [81], © American Chemical Society 2025. (c) DEMS spectra of Ru-LCN for NORR at −0.2 V vs. RHE. Reproduced with permission from Ref. [32], © American Chemical Society 2022. (d) The ^{1}H NMR spectra obtained from ^{15}NO, NO, and Ar for NORR. Reproduced with permission from Ref. [82], © Yang, W. et al. 2025. (e) Heatmap of *operando* EPR spectra during the NORR process. Reproduced with permission from Ref. [81], © American Chemical Society 2025. (f) Schematic diagram of *in situ* IR reaction cell. Reproduced with permission from Ref. [84], © American Chemical Society 2024. (g) *In situ* IR spectra of NO reduction on Cu (111) catalyst. Reproduced with permission from Ref. [62], © Wiley-VCH GmbH 2024.

3.4.2 *Theoretical calculation*

Density functional theory (DFT) calculations provide indispensable atomic-scale insights that complement experimental observations [68, 85–90]. By evaluating electronic structures, intermediate adsorption energies, and reaction barriers, DFT clarifies the potential functions of active sites and predicts feasible reaction pathways, providing support for experimental observations. For instance, volcano plots relating limiting potentials and the RDS enable rapid assessment of catalytic performance, facilitating the identification of promising catalysts. Moreover, to further streamline catalyst screening, adsorption-energy scaling relations are employed to establish descriptor-based approaches. In a study by Long et al., the N* adsorption free energy (G_{ad}(N)) served as a core descriptor to calculate adsorption energies of all intermediates involved in NORR, NRR, and HER across ten transition-metal catalysts [40]. The descriptor-based strategy facilitates screening of catalysts with high activity along specific reaction pathways and enables assessment of activity across multiple mechanisms.

In summary, the synergistic integration of multiscale *in situ* characterization and DFT modeling has profoundly advanced the mechanistic understanding of NORR. Future research should therefore focus on developing innovative *in situ* characterization techniques with higher resolution, sensitivity, and adaptability that can be integrated into multi-technique platforms for real-time monitoring of active-site evolution and intermediate dynamics. On the theoretical side, further progress requires moving beyond static

analysis toward integrated multiscale modeling frameworks with first-principles molecular dynamics, microkinetic simulations, and data-driven machine learning approaches. Coupling these advanced computational approaches with higher-resolution *operando* experiments will be crucial for mapping the complete energy landscape of NORR and guiding the rational design of high-performance catalysts.

4 Reaction systems

The practical application of NORR is highly dependent on the reaction environment, and the systems can be primarily classified into two widely investigated configurations based on mass transfer modes, reactant supply forms, and catalytic interface characteristics: gas–liquid–solid triphase interfacial systems and gas–solid systems. Each configuration exhibits distinct interfacial properties, active-site exposure, and product distributions, thereby imposing different requirements on catalyst design and reaction condition optimization.

4.1 Gas–liquid–solid triphase interface system

In NORR, the gas–liquid–solid three-phase interface represents a typical reaction environment, where NO dissolves into the liquid phase and undergoes reduction at the catalyst interface. A key advantage of the gas–liquid–solid triphase interface is the coupling of dissolved NO molecules with proton migration in the solution phase, which facilitates electron–proton pair transfer. However, the solubility of NO in water is limited to 1.8 mmol·dm^{-3}, restricting both reaction concentration and mass transfer efficiency. Therefore, enhancing the effective supply of NO in the liquid phase remains a primary challenge in gas–liquid–solid systems. To overcome the bottleneck in NO effective supply, chemical and physical strategies have been developed.

Chemical strategies to enhance NO solubility. Metal complexes can be introduced into the solution phase to increase NO solubility, providing sufficient reactants for subsequent NORR. Ethylenediaminetetraacetic acid (EDTA) chelate solutions are widely employed to increase NO concentration in the liquid phase by forming stable complexes with NO molecules [27, 31, 63]. Li et al. employed Fe(II)-EDTA solution as an absorbent to achieve efficient NO capture and transfer [91]. Experimental results (Figs. 6(a) and 6(b)) indicate that in the absence of Fe(II)-EDTA, the –NH characteristic peak is weak, whereas the introduction of Fe(II)-EDTA significantly increases peak intensity, demonstrating

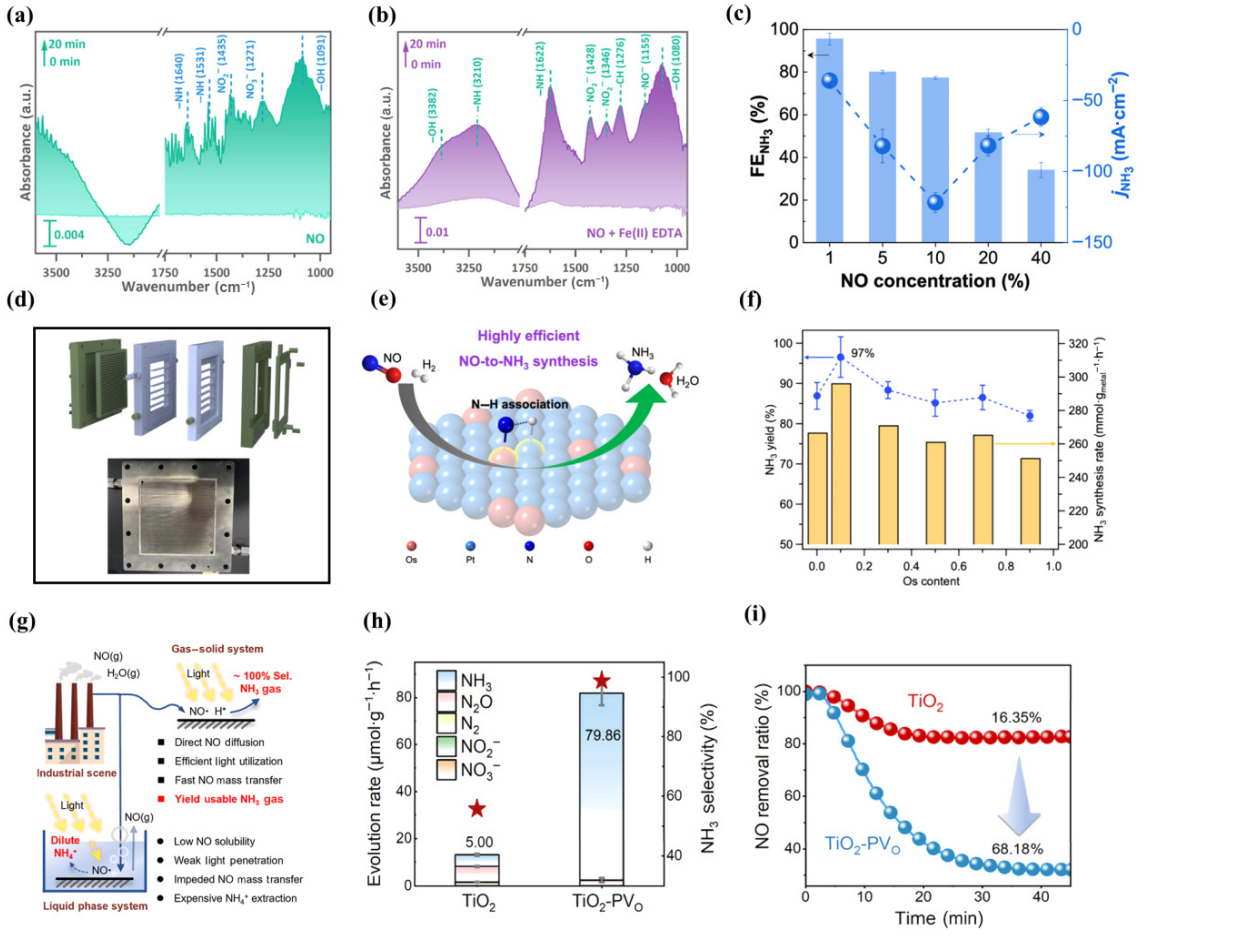

Figure 6 ((a) and (b)) *In situ* liquid-phase diffuse reflectance infrared Fourier transform spectroscopy (DRIFTS) spectra for NO reduction without (a) or with Fe(II)-EDTA (b). ((a) and (b)) Reproduced with permission from Ref. [91], © American Chemical Society 2023. (c) Faradaic efficiencies of NH_3 at –0.6 V vs. RHE under different NO concentrations. Reproduced with permission from Ref. [92], © American Chemical Society 2022. (d) Schematic of the flow cell equipped with a serpentine runner Ti plate. Reproduced with permission from Ref. [62], © Wiley-VCH GmbH 2024. (e) Schematic illustration of efficient NO to ammonia synthesis. (f) NH_3 yield of the catalyst at 200 °C and ambient pressure. Reproduced with permission from Ref. [93], © American Chemical Society 2025. (g) Comparison of key features and distinctions between gas–solid and gas–liquid–solid multiphase catalytic pathways for NO-to-NH_3 conversion. (h) Products yield and selectivity. (i) NO conversion efficiency. ((g)–(i)) Reproduced with permission from Ref. [81], © American Chemical Society 2025.

effective conversion of NO to NH_4^+. Continuous absorption and conversion of NO results in a NO conversion efficiency of 89.05% ± 0.71%. However, chemical strategies introduce higher operational costs, increase reaction complexity, and may influence product selectivity.

Complementary to chemical approaches, physical strategies aim to improve NO transport in the liquid phase and mitigate the limitations of low solubility. A common method involves increasing the NO concentration in the reaction atmosphere (> 10,000 ppm or pure NO gas), which accelerates gas–liquid interfacial transfer and partially enhances reaction efficiency. However, such high NO concentration releases large amounts of unconverted NO, resulting in resource loss and potential environmental pollution. Moreover, high NO concentration deviates from practical scenarios, where NO typically originates from dilute sources, such as industrial flue gas, limiting applicability. To address these challenges, strategies based on electrode and reactor design have been proposed. Cheon et al. developed a gas diffusion electrode (GDE) that shortened the gas diffusion pathway and enlarged the gas-catalyst contact area [92], enabling low-concentration NO (1%–10%) to participate in electrochemical reactions without complete dissolution in the electrolyte. When converting 1% NO, the Faradaic efficiency reached 96% (Fig. 6(c)), demonstrating effective adaptation to dilute feeds. Xiao et al. further optimized the reaction configuration employing a flow cell equipped with a 1 cm × 1 cm and 5 cm × 5 cm serpentine runner Ti plate and a GDE (Fig. 6(d)), which facilitated NO diffusion at the catalyst surface and improved mass exchange with the flowing phase [62]. In addition, a polyvinylidene fluoride (PVDF) coating enhanced hydrophobicity and gas affinity, optimizing NO diffusion pathways and reducing resistance from the aqueous phase. Under near-neutral electrolyte conditions, NO conversion reached 63.74%, representing the highest efficiency reported for electrocatalytic NORR to date. Although physical strategies have improved NO mass transfer and conversion efficiency, further optimization of electrode architecture, interfacial properties, and reactor design is required to approach industrial-scale conversion.

In addition to limitations in solubility and mass transfer, the gas–liquid–solid triphase system faces challenges in product recovery, as it primarily yields low concentrations of NH_4^+ rather than NH_3, which can be directly stored and transported, thereby necessitating additional separation and purification steps. Current industrial methods for ammonia separation include condensation, absorption, and membrane separation. Condensation enables high-purity recovery but is energy-intensive and requires harsh operating conditions. Absorption often introduces additional separation steps, increasing energy consumption and potential secondary pollution. Membrane separation offers high selectivity but is costly, with limited durability for membrane materials. Given these limitations, gas–solid systems have attracted increasing attention, as they circumvent the solubility and separation constraints of liquid-phase environments, opening new avenues for efficient and sustainable NORR.

4.2 Gas–solid system

Gas–solid systems allow NO molecules to directly interact with the catalyst surface, bypassing dissolution processes in the liquid phase. This configuration eliminates solubility-related limitations and reduces reliance on complex reactor designs. Efficient NO reduction can be achieved even under low-concentration feeds, better simulating industrial flue gas conditions. Moreover, when conversion and selectivity approach 100%, the generated NH_3 gas can be directly collected in the gas phase, avoiding extracting dilute NH_4^+ from aqueous systems and substantially lowering energy and operational demands.

In contrast to liquid-phase catalytic systems, where protons are readily available, gaseous H_2O molecules lack solvation and hydrogen-bonding interactions. Consequently, H_2O dissociation at the gas–solid interface exhibits an energy barrier (> 420 kJ·mol^{-1}), which is higher than that in liquid H_2O (~ 100 kJ·mol^{-1}), leading to inefficient proton supply and limiting both conversion efficiency and product selectivity. The insufficient proton supply thus represents a key limitation in gas–solid NORR for ammonia synthesis, hindering reaction efficiency and leading to relatively few studies in this field. To address this issue, Qin et al. employed H_2 as a proton source (Fig. 6(e)), where H_2 dissociation generates surface H* to facilitate NO reduction and hydrogenation, achieving an NH_3 yield of up to 97% (Fig. 6(f)) [93]. However, the reaction also requires heating to 200 °C and depends on externally supplied H_2, which is not present in typical industrial flue gas streams. The external H_2 further increases system complexity and cost. Therefore, developing greener, more energy-efficient, and practically relevant reaction conditions remains essential for realizing ammonia synthesis via NORR.

Photocatalytic NORR to ammonia using water as the proton source operates under ambient temperature and pressure, reducing feedstock costs and improving sustainability. To overcome the limitation of insufficient proton supply in gas–solid systems, Sheng et al. developed a gas–solid photocatalytic NORR system on TiO_2 with PV_O to facilitate H_2O activation [81]. PV_O modulates the dynamic electronic structure, allowing electrons to occupy deep conduction band states and generate high-energy carriers, which promote H_2O dissociation and ensure a stable proton supply (Fig. 6(g)). The optimized TiO_2-PV_O catalyst achieved an NH_3 yield of 79.86 ± 3.48 μmol·g^{-1}·h^{-1} with nearly 100% selectivity (Fig. 6(h)) and an NO conversion efficiency of 68.18% (Fig. 6(i)). This work demonstrates the potential of photocatalytic NORR as a pathway for sustainable ammonia synthesis, although further optimization of proton supply and NO conversion efficiency is required to achieve practical and scalable ammonia production under gas–solid conditions.

5 NORR to ammonia from industrial flue gas sources

Most reported NORR studies have been conducted using pure NO or high NO concentration (> 10 vol.%), far exceeding the levels typically present in industrial flue gas (500–1000 ppm) [35, 45, 61, 63, 94]. Such low NO concentration weakens surface coverage and slows reaction kinetics, posing significant challenges for efficient adsorption, activation, and reduction [32, 42, 51, 95–99]. To overcome these limitations, various strategies have been employed to enhance NO adsorption and activation, lower reaction barriers, and suppress competing byproduct formation.

Structural tuning, such as reducing metal coordination numbers and strengthening metal–support interactions, can effectively modulate the electronic structure, thereby improving NORR performance [95]. For example, Li et al. prepared Ru nanosheets with low coordination number (Ru-LCN) via plasma treatment of high coordination Ru precursors (Fig. 7(a)) [32]. At −0.2 V vs.

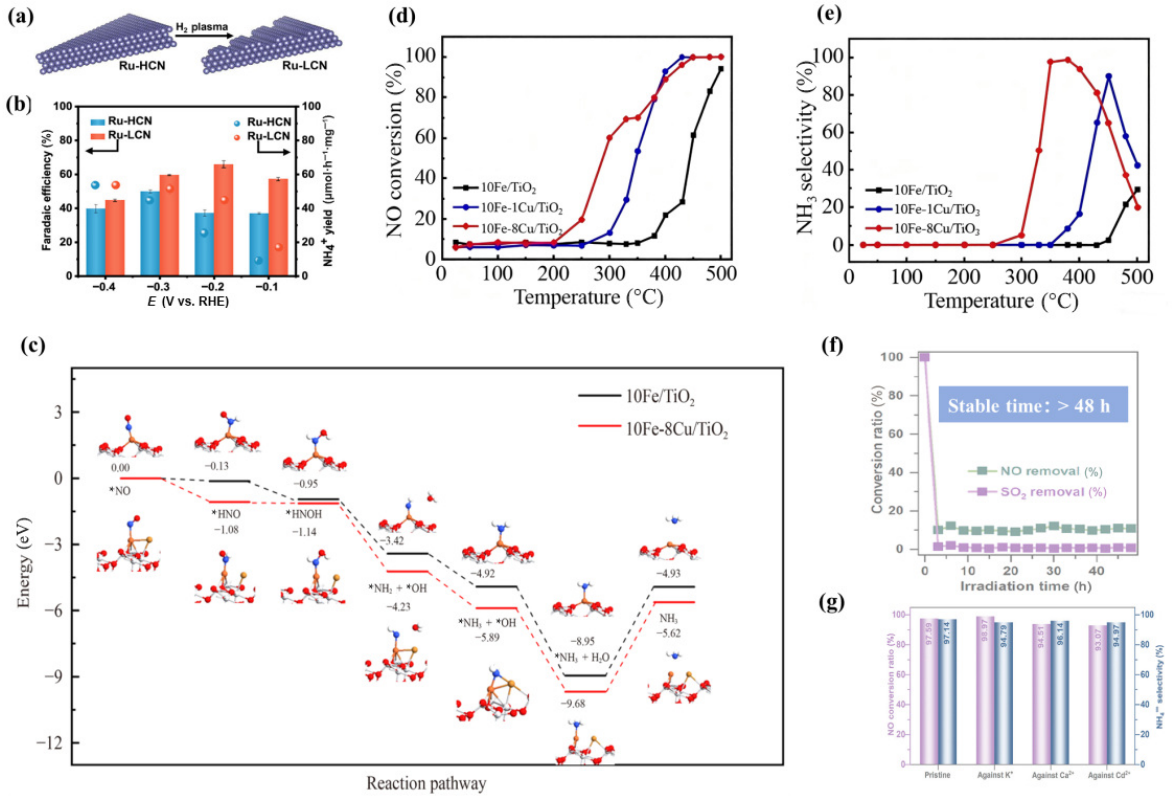

Figure 7 (a) Schematic illustration of Ru-high coordination number (Ru-HCN) and Ru-LCN. (b) Faradaic efficiency and NH_4^+ yield with 1% NO reduction over Ru-HCN and Ru-LCN at each given potential. ((a) and (b)) Reproduced with permission from Ref. [32], © American Chemical Society 2022. (c) Schematic of NO reduction pathways on 10Fe/TiO_2 (black) and 10Fe-8Cu/TiO_2 (red). (d) NO conversion efficiency of the catalysts. (e) NH_3 selectivity of the catalysts. ((c)–(e)) Reproduced with permission from Ref. [100], © Higher Education Press 2023. (f) Catalytic activity under continuous NO and SO_2 conversion. (g) Poisoning resistance of the catalyst against coexisting metal ions in the flue gas. ((f) and (g)) Reproduced with permission from Ref. [101], © American Chemical Society 2023.

RHE, the Ru-LCN achieved a Faradaic efficiency of 65.96% and an NH_4^+ yield rate of 45.02 μmol·h^{-1}·mg^{-1} under 1% NO (~ 10,000 ppm) (Fig. 7(b)). Although this design significantly improved activity, the operating NO concentration remains far above industrial flue gas levels, indicating that efficient NORR under truly dilute conditions is still difficult to achieve.

In contrast, gas–solid catalytic systems have shown greater potential for low-concentration NO utilization by bypassing solubility limitations and enabling direct gas catalyst interactions. A representative example is the Cu-doped Fe/TiO_2 catalyst, in which Cu incorporation enhances NO adsorption, lowers the energy barrier of the RDS (*NO → *NHO), and facilitates NH_3 desorption (Fig. 7(c)) [100]. Under simulated flue gas conditions containing only 350 ppm NO, this system achieved over 80% NO conversion and more than 98% NH_3 selectivity (Figs. 7(d) and 7(e)), highlighting the feasibility of selective ammonia synthesis from dilute NO streams.

Beyond low NO concentrations, the complex composition of industrial flue gas introduces additional difficulties. Coexisting species, such as SO_2, CO_2, volatile organic compounds (VOCs), and particulates, can compete for active sites, alter surface chemistry, or induce catalyst deactivation. Interestingly, some components traditionally regarded as poisons may play constructive roles when properly integrated into the reaction system. For instance, SO_2 has been shown to function as a redox partner in coupled NORR processes, enabling direct ammonia synthesis from mixed flue gas while simultaneously enhancing resistance to catalyst poisoning and facilitating heavy-metal removal (Figs. 7(f) and 7(g)) [101]. These findings illustrate that flue-gas components can exert multifaceted effects on NORR and should be considered collectively rather than individually.

From a broader perspective, practical NORR applications must operate under stringent industrial constraints, including dilute NO concentrations, coexisting reactive species (e.g., O_2, SO_2, and H_2O), fluctuating operating conditions, and long-term stability requirements. Under such conditions, catalyst performance can no longer be optimized based on a single metric. Instead, rational catalyst design should follow overarching mechanistic principles that enable the simultaneous optimization of activity, selectivity, poisoning resistance, and durability. Catalysts suitable for realistic flue gas environments should be capable of operating efficiently under low-coverage regimes, exhibit moderate adsorption strengths, and possess electronically adaptive active sites that can respond to dynamic reaction environments.

In summary, under such complex industrial flue gas environments, NORR catalyst performance can no longer be optimized based on a single metric, but instead requires a coordinated balance among activity, selectivity, poisoning resistance, and long-term durability [102–105]. Based on the mechanistic insights and representative case studies discussed above, the following key design principles can be distilled:

(1) Efficient activation under low-coverage conditions. Active sites should possess high intrinsic affinity and reaction specificity toward NO molecules, enabling the preferential capture and activation of ppm-level NO even in the presence of competitive species, such as O_2 and H_2O.

(2) Moderation of adsorption strength. Through the synergistic tuning of electronic structure and geometric configuration, the adsorption energies of key intermediates (e.g., *NO and *NHO) should be regulated within an optimal window that is neither too strong nor too weak, thereby balancing activation, transformation efficiency, and resistance to catalyst poisoning.

(3) Dynamic electronic adaptability. Active centers should be capable of responding to fluctuations in flue gas composition and operating conditions, maintaining favorable reaction pathways, and ensuring stable operation under realistic environments.

These principles not only provide guidance for rational catalyst design at the atomic scale, but also offer system-level implications for reactor configuration and operational strategies, such as enhancing gas–solid contact and mass transport through reactor engineering, utilizing waste heat in flue gas to improve reaction kinetics, and managing the influence of complex components through integrated system control. By explicitly linking microscopic mechanistic understanding with macroscopic engineering constraints, these principles establish a conceptual framework for translating laboratory-scale high-performance materials into practically viable NORR technologies. Although further investigations are still required to address long-term durability and complex deactivation pathways, this principle-driven design strategy provides a critical rational foundation for the development of NORR catalysts and systems tailored to realistic flue gas environments.

6 Summary and perspectives

In summary, despite significant progress in fundamental research on NORR for ammonia synthesis, most studies remain laboratory-scale and rely on idealized conditions. To advance NORR to industrial application, targeted improvements are required in reaction system engineering, adaptability to complex operating conditions, energy efficiency, and characterization methods (Fig. 8). From a practical perspective, progress toward application is generally associated with achieving high NH_3 selectivity, sustained NH_3 production under dilute NO conditions, and stable operation over extended periods under realistic reaction environments. Future research priorities are as follows:

(1) Photothermal synergistic systems. Photothermal strategies enable the utilization of waste heat in industrial flue gas, providing complementary benefits for energy utilization and reaction efficiency. Future efforts should focus on optimizing reactor configurations for light-heat transfer, regulating field distributions, and elucidating coupling mechanisms between photogenerated carriers and thermally activated reactants.

(2) Catalytic systems for low-concentration NO in complex atmospheres. Industrial flue gas has low NO concentrations and additional components, including O_2, SO_2, CO_2, VOCs, and particulates, which compete for electrons or active sites and potentially induce catalyst poisoning. Future research should systematically evaluate catalytic systems under simulated industrial conditions (complex mixtures, fluctuating parameters, variable NO concentrations), elucidating activity, selectivity, and stability, and developing catalytic systems with strong NO adsorption, activation, anti-poisoning ability, and robust selectivity.

(3) Gas–solid systems and the protonation bottleneck. Gas–solid systems are promising for industrial use, owing to compatibility with industrial flue gas, high NO mass transfer, no sacrificial agents, efficient light utilization, and no extra product separation. However, limited proton transfer restricts the reaction rate and NH_3 selectivity. Addressing this challenge involves tuning catalyst electronic structures, constructing efficient water dissociation sites, and designing electron–proton co-transport pathways to enhance proton supply and transfer efficiency, thereby facilitating efficient NH_3 production.

(4) Advanced *in situ* characterization and mechanism. NORR involves complex pathways and transient intermediates, but the mechanism remains insufficiently understood. Current characterization techniques exhibit limited temporal and spatial resolution, restricting precise identification of key intermediates. Developing high-resolution *in situ* techniques for real-time intermediate monitoring to clarify mechanisms and guide catalyst design. Combining complementary *in situ* techniques, including Raman-IR and EPR spectroscopy coupling, helps capture transient species, enabling a comprehensive understanding of structure–performance–kinetics relationships in NORR.

(5) Artificial intelligence-assisted catalyst design. Artificial intelligence and machine learning accelerate NORR catalyst development via high-throughput screening and structure–performance prediction. Integrating experimental databases with theoretical calculations to build predictive models for low-concentration NO activation and high NH_3 selectivity. High-throughput computations combined with machine learning systematically explore correlations between active site properties (oxidation state, coordination number, defects) and performance, guiding rational design of innovative and efficient catalysts for NORR to ammonia synthesis.

Data availability

Not applicable.

Acknowledgements

This work was supported by the National Natural Science

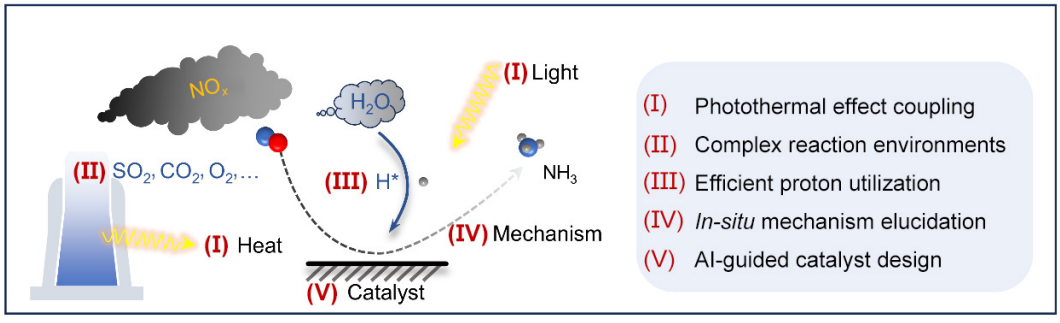

Figure 8 Key future research priorities for developing efficient and practical ammonia synthesis from NO.

Foundation of China (Nos. 22506015, 22522601, 22361142703, and 22225606), the Sichuan Science and Technology Program (Nos. 2026NSFSC0874 and 2025NSFTD0003), the China Postdoctoral Science Foundation (No. 2025M771224), and the Postdoctoral Fellowship Program of CPSF under Grant (No. GZB20250309).

Declaration of competing interest

All the contributing authors report no conflict of interests in this work.

Author contribution statement

Y. H.: Conceptualization, writing manuscript. H. Q. J.: Writing manuscript. J. P. S.: Writing manuscript, revision. F. D.: Project administration, supervision. Y. J. S.: Writing manuscript, revision. All the authors have approved the final manuscript.

Use of AI statement

During the preparation of this work, the authors used ChatGPT only for language polishing and correction of grammatical errors. After using this tool, the authors reviewed and edited the content as needed and take full responsibility for the content of the publication.

References

[1] Anenberg, S. C.; Miller, J.; Minjares, R.; Du, L.; Henze, D. K.; Lacey, F.; Malley, C. S.; Emberson, L.; Franco, V.; Klimont, Z. et al. Impacts and mitigation of excess diesel-related NO_x emissions in 11 major vehicle markets. *Nature* **2017**, *545*, 467–471.

[2] Gruber, N.; Galloway, J. N. An Earth-system perspective of the global nitrogen cycle. *Nature* **2008**, *451*, 293–296.

[3] Felix, J. D.; Elliott, E. M.; Shaw, S. L. Nitrogen isotopic composition of coal-fired power plant NO_x: Influence of emission controls and implications for global emission inventories. *Environ. Sci. Technol.* **2012**, *46*, 3528–3535.

[4] Lelieveld, J.; Evans, J. S.; Fnais, M.; Giannadaki, D.; Pozzer, A. The contribution of outdoor air pollution sources to premature mortality on a global scale. *Nature* **2015**, *525*, 367–371.

[5] Richter, A.; Burrows, J. P.; Nüß, H.; Granier, C.; Niemeier, U. Increase in tropospheric nitrogen dioxide over China observed from space. *Nature* **2005**, *437*, 129–132.

[6] Shan, Y. L.; Du, J. P.; Zhang, Y.; Shan, W. P.; Shi, X. Y.; Yu, Y. B.; Zhang, R. D.; Meng, X. J.; Xiao, F. S.; He, H. Selective catalytic reduction of NO_x with NH_3: Opportunities and challenges of Cu-based small-pore zeolites. *Natl. Sci. Rev.* **2021**, *8*, nwab010.

[7] Chen, W.; Yang, S.; Liu, H.; Huang, F.; Shao, Q. H.; Liu, L. C.; Sun, J. F.; Sun, C. Z.; Chen, D. Z.; Dong, L. Single-atom Ce-modified α-Fe_2O_3 for selective catalytic reduction of NO with NH_3. *Environ. Sci. Technol.* **2022**, *56*, 10442–10453.

[8] Shi, Z. W.; Peng, Q. G.; E, J. Q.; Xie, B.; Wei, J.; Yin, R. X.; Fu, G. Mechanism, performance and modification methods for NH_3-SCR catalysts: A review. *Fuel* **2023**, *331*, 125885.

[9] Ma, L.; Li, J. H.; Cheng, Y. S.; Lambert, C. K.; Fu, L. X. Propene poisoning on three typical Fe-zeolites for SCR of NO_x with NH_3: From mechanism study to coating modified architecture. *Environ. Sci. Technol.* **2012**, *46*, 1747–1754.

[10] Chen, W. B.; Zou, R. Q.; Wang, X. D. Toward an atomic-level understanding of the catalytic mechanism of selective catalytic reduction of NO_x with NH_3. *ACS Catal.* **2022**, *12*, 14347–14375.

[11] Zhang, R. D.; Liu, N.; Lei, Z. G.; Chen, B. H. Selective transformation of various nitrogen-containing exhaust gases toward N_2 over zeolite catalysts. *Chem. Rev.* **2016**, *116*, 3658–3721.

[12] Han, L. P.; Cai, S. X.; Gao, M.; Hasegawa, J. Y.; Wang, P. L.; Zhang, J. P.; Shi, L. Y.; Zhang, D. S. Selective catalytic reduction of NO_x with NH_3 by using novel catalysts: State of the art and future prospects. *Chem. Rev.* **2019**, *119*, 10916–10976.

[13] Chen, R. M.; Wang, J. L.; Zhang, C. L.; Sun, Y. J.; Li, J. Y.; Dong, F. Purification and value-added conversion of NO_x under ambient conditions with photo-/electrocatalysis technology. *Environ. Sci. Technol.* **2025**, *59*, 1013–1033.

[14] Wang, D. D.; Lu, X. F.; Luan, D. Y.; Lou, X. W. Selective electrocatalytic conversion of nitric oxide to high value-added chemicals. *Adv. Mater.* **2024**, *36*, 2312645.

[15] Bertagni, M. B.; Socolow, R. H.; Martirez, J. M. P.; Carter, E. A.; Greig, C.; Ju, Y. G.; Lieuwen, T.; Mueller, M. E.; Sundaresan, S.; Wang, R. et al. Minimizing the impacts of the ammonia economy on the nitrogen cycle and climate. *Proc. Natl. Acad. Sci. USA* **2023**, *120*, e2311728120.

[16] Li, S. F.; Zhou, Y. Y.; Fu, X. B.; Pedersen, J. B.; Saccoccio, M.; Andersen, S. Z.; Enemark-Rasmussen, K.; Kempen, P. J.; Damsgaard, C. D.; Xu, A. N. et al. Long-term continuous ammonia electrosynthesis. *Nature* **2024**, *629*, 92–97.

[17] Foster, S. L.; Bakovic, S. I. P.; Duda, R. D.; Maheshwari, S.; Milton, R. D.; Minteer, S. D.; Janik, M. J.; Renner, J. N.; Greenlee, L. F. Catalysts for nitrogen reduction to ammonia. *Nat. Catal.* **2018**, *1*, 490–500.

[18] Ashida, Y.; Arashiba, K.; Nakajima, K.; Nishibayashi, Y. Molybdenum-catalysed ammonia production with samarium diiodide and alcohols or water. *Nature* **2019**, *568*, 536–540.

[19] Hu, H.; Pan, S. Y.; Ma, Z. Y.; Liu, K. Y.;Bao, H. F.; Deng, C. W.; Luo. F.; Yang. Z. H. A self-powered system to electrochemically generate ammonia driven by palladium single atom electrocatalyst. *SusMat* **2024**, *4*, e237.

[20] Chen, J. G.; Crooks, R. M.; Seefeldt, L. C.; Bren, K. L.; Bullock, R. M.; Darensbourg, M. Y.; Holland, P. L.; Hoffman, B.; Janik, M. J.; Jones, A. K. et al. Beyond fossil fuel-driven nitrogen transformations. *Science* **2018**, *360*, eaar6611.

[21] Soloveichik, G. Electrochemical synthesis of ammonia as a potential alternative to the Haber–Bosch process. *Nat. Catal.* **2019**, *2*, 377–380.

[22] Yang, X. X.; Mukherjee, S.; O'Carroll, T.; Hou, Y.; Singh, M. R.; Gauthier, J. A.; Wu, G. Achievements, challenges, and perspectives on nitrogen electrochemistry for carbon-neutral energy technologies. *Angew. Chem., Int. Ed.* **2023**, *62*, e202215938.

[23] Wang, T.; Abild-Pedersen, F. Achieving industrial ammonia synthesis rates at near-ambient conditions through modified scaling relations on a confined dual site. *Proc. Natl. Acad. Sci. USA* **2021**, *118*, e2106527118.

[24] Green ammonia synthesis. *Nat. Synth.* **2023**, *2*, 581–582.

[25] Huang, Z. L.; Rafiq, M.; Woldu, A. R.; Tong, Q. X.; Astruc, D.; Hu, L. S. Recent progress in electrocatalytic nitrogen reduction to ammonia (NRR). *Coord. Chem. Rev.* **2023**, *478*, 214981.

[26] Huang, P. W.; Hatzell, M. C. Prospects and good experimental practices for photocatalytic ammonia synthesis. *Nat. Commun.* **2022**, *13*, 7908.

[27] Liu, P. Y.; Liang, J.; Wang, J. Q.; Zhang, L. C.; Li, J.; Yue, L. C.; Ren, Y. C.; Li, T. S.; Luo, Y. L.; Li, N. et al. High-performance NH_3 production via NO electroreduction over a NiO nanosheet array. *Chem. Commun.* **2021**, *57*, 13562–13565.

[28] Liu, D.; Chen, M. P.; Du, X. Y.; Ai, H. Q.; Lo, K. H.; Wang, S. P.; Chen, S.; Xing, G. C.; Wang, X. S.; Pan, H. Development of electrocatalysts for efficient nitrogen reduction reaction under ambient condition. *Adv. Funct. Mater.* **2021**, *31*, 2008983.

[29] Chen, K.; Wang, F. Z.; Lu, X. B.; Li, Y. H.; Chu, K. Atomically

dispersed W_1–O_3 bonded on Pd metallene for cascade NO electroreduction to NH_3. *ACS Catal.* **2023**, *13*, 9550–9557.

[30] Dhanabal, D.; Markandaraj, S. S.; Shanmugam, S. Transition metal nanoparticle-embedded nitrogen-doped carbon nanorods as an efficient electrocatalyst for selective electroreduction of nitric oxide to ammonia. *ACS Catal.* **2023**, *13*, 9136–9149.

[31] Kim, D. Y.; Shin, D.; Heo, J.; Lim, H.; Lim, J. A.; Jeong, H. M.; Kim, B. S.; Heo, I.; Oh, I.; Lee, B. et al. Unveiling electrode–electrolyte design-based NO reduction for NH_3 synthesis. *ACS Energy Lett.* **2020**, *5*, 3647–3656.

[32] Li, Y. B.; Cheng, C. Q.; Han, S. H.; Huang, Y. M.; Du, X. W.; Zhang, B.; Yu, Y. F. Electrocatalytic reduction of low-concentration nitric oxide into ammonia over Ru nanosheets. *ACS Energy Lett.* **2022**, *7*, 1187–1194.

[33] Fan, X. X.; Teng, Z. Y.; Han, L. P.; Shen, Y. J.; Wang, X. Y.; Qu, W. Q.; Song, J. L.; Wang, Z. L.; Duan, H. Y.; Wu, Y. A. et al. Boosted charge and proton transfer over ternary Co/Co_3O_4/CoB for electrochemical nitric oxide reduction to ammonia. *Nat. Commun.* **2025**, *16*, 4874.

[34] Wang, Z. L.; Duan, H. Y.; Qu, W. Q.; Zhang, H.; Han, L. P.; Teng, Z. Y.; Chen, G. R.; Cheng, D. H.; Wang, X. Y.; Wu, Y. A. et al. Regulating local reaction environments for efficient nitric oxide reduction to ammonia via strengthening interactions between heteroatom-doped carbon and metallic alloys. *Adv. Funct. Mater.* **2025**, *35*, 2507533.

[35] Bai, C. P.; Wang, J.; Fan, S. Y.; Li, X. Y.; Liu, S. M. Modulating the reorientation of interfacial water to promote electrochemical NO reduction to NH_3 on palladium-copper catalysts. *ACS Catal.* **2025**, *15*, 9442–9451.

[36] Liu, H.; Wu, L.; Fu, Y. X.; Wang, Z. J.; Long, J. Q.; Yuan, J.; Wang, X. L.; Li, J. Y.; Wu, J.; Xiang, K. S. Promotion of nitric oxide to ammonia via nickel species enhanced active hydrogen generation. *Chem. Eng. J.* **2026**, *527*, 171687.

[37] Han, D. L.; Wang, Z. L.; Duan, H. Y.; Yang, L. P.; Zhang, H.; Mariani, E.; Gao, M. D.; Wei, Z. Q.; Li, X. C.; Han, L. P. et al. Molecularly engineered co-phthalocyanine covalent organic frameworks for efficient nitric oxide-to-ammonia electroreduction. *J. Am. Chem. Soc.* **2025**, *147*, 41355–41366.

[38] Markandaraj, S. S.; Muthusamy, T.; Shanmugam, S. Electrochemical reduction of nitric oxide with 1.7% solar-to-ammonia efficiency over nanostructured core–shell catalyst at low overpotentials. *Adv. Sci.* **2022**, *9*, 2201410.

[39] Meng, G.; Wei, T. R.; Liu, W. J.; Li, W. B.; Zhang, S. S.; Liu, W. X.; Liu, Q.; Bao, H. H.; Luo, J.; Liu, X. J. NiFe layered double hydroxide nanosheet array for high-efficiency electrocatalytic reduction of nitric oxide to ammonia. *Chem. Commun.* **2022**, *58*, 8097–8100.

[40] Long, J.; Chen, S. M.; Zhang, Y. L.; Guo, C. X.; Fu, X. Y.; Deng, D. H.; Xiao, J. P. Direct electrochemical ammonia synthesis from nitric oxide. *Angew. Chem., Int. Ed.* **2020**, *59*, 9711–9718.

[41] Chen, K.; Shen, P.; Zhang, N. N.; Ma, D. W.; Chu, K. Electrocatalytic NO reduction to NH_3 on Mo_2C nanosheets. *Inorg. Chem.* **2023**, *62*, 653–658.

[42] Wang, D. D.; Fan, G. L.; Luan, D. Y.; Guo, Y.; Gu, X. J.; Lou, X. W. Ru-incorporation-induced phase transition in co nanoparticles for low-concentration nitric oxide electroreduction to ammonia at low potential. *Adv. Mater.* **2024**, *36*, 2408580.

[43] Zhang, H. F.; Li, Y. B.; Cheng, C. Q.; Zhou, J.; Yin, P. F.; Wu, H. M.; Liang, Z. Q.; Zhang, J. W.; Yun, Q. B.; Wang, A. L. et al. Isolated electron-rich ruthenium atoms in intermetallic compounds for boosting electrochemical nitric oxide reduction to ammonia. *Angew. Chem., Int. Ed.* **2023**, *62*, e202213351.

[44] Wang, D. D.; Chen, Z. W.; Gu, K. Z.; Chen, C.; Liu, Y. Y.; Wei, X. X.; Singh, C. V.; Wang, S. Y. Hexagonal cobalt nanosheets for high-performance electrocatalytic NO reduction to NH_3. *J. Am. Chem. Soc.* **2023**, *145*, 6899–6904.

[45] Zhao, S. W.; Liu, J. Y.; Zhang, Z. B.; Zhu, C. Y.; Shi, G. S.; Wu, J.; Yang, C. L.; Wang, Q. H.; Chang, M. W.; Liu, K. H. et al. Deciphering nickel-catalyzed electrochemical ammonia synthesis from nitric oxide. *Chem* **2023**, *9*, 3555–3572.

[46] Li, Z. X.; Zhou, Q.; Liang, J.; Zhang, L. C.; Fan, X. Y.; Zhao, D. L.; Cai, Z. W.; Li, J.; Zheng, D. D.; He, X. et al. Defective TiO_{2-x} for high-performance electrocatalytic NO reduction toward ambient NH_3 production. *Small* **2023**, *19*, 2300291.

[47] He, C. Z.; Sun, R. S.; Fu, L.; Huo, J. R.; Zhao, C. X.; Li, X. Y.; Song, Y.; Wang, S. M. Defect engineering for high-selection-performance of NO reduction to NH_3 over CeO_2 (111) surface: A DFT study. *Chin. Chem. Lett.* **2022**, *33*, 527–532.

[48] Linling, G.; Liao, Z.; Zhang, H. M.; Jiang, J. X.; Chen, Z. K. From defects to catalysis: Mechanism and optimization of NO electroreduction synthesis of NH_3. *Front. Chem.* **2024**, *12*, 1452689.

[49] Bai, S.; Zhang, N.; Gao, C.; Xiong, Y. J. Defect engineering in photocatalytic materials. *Nano Energy* **2018**, *53*, 296–336.

[50] Kang, X. X.; Fang, Q. C.; Yin, H. Q.; Du, A. J.; Duan, X. M. Enhancing electrocatalytic nitrate/nitric oxide reduction to NH_3 on two-dimensional p-block InSe monolayer via defect engineering. *Mol. Catal.* **2024**, *568*, 114477.

[51] Guo, X. X.; Wang, P.; Wu, T. W.; Wang, Z. Q.; Li, J.; Liu, K.; Fu, J. W.; Liu, M.; Wu, J.; Lin, Z. et al. Aqueous electroreduction of nitric oxide to ammonia at low concentration via vacancy engineered FeOCl. *Angew. Chem., Int. Ed.* **2024**, *63*, e202318792.

[52] Zhang, B. K.; Dai, Y.; Huang, B. B.; Qian, Z.; Ahuja, R.; Wei, W. Improving nitric oxide reduction reaction through surface doping on superstructures. *Nano Energy* **2024**, *123*, 109396.

[53] Chen, K.; Zhang, Y.; Xiang, J. Q.; Zhao, X. L.; Li, X. G.; Chu, K. p-Block antimony single-atom catalysts for nitric oxide electroreduction to ammonia. *ACS Energy Lett.* **2023**, *8*, 1281–1288.

[54] Guo, W. X.; Wang, Z. Y.; Wang, X. Q.; Wu, Y. E. General design concept for single-atom catalysts toward heterogeneous catalysis. *Adv. Mater.* **2021**, *33*, 2004287.

[55] Chen, K.; Zhang, G. K.; Li, X. T.; Zhao, X. L.; Chu, K. Electrochemical NO reduction to NH_3 on Cu single atom catalyst. *Nano Res.* **2023**, *16*, 5857–5863.

[56] Peng, X. Y.; Mi, Y. Y.; Bao, H. H.; Liu, Y. F.; Qi, D. F.; Qiu, Y.; Zhuo, L. C.; Zhao, S. Z.; Sun, J. Q.; Tang, X. L. et al. Ambient electrosynthesis of ammonia with efficient denitration. *Nano Energy* **2020**, *78*, 105321.

[57] Chen, K.; Wang, J. X.; Kang, J. L.; Lu, X. B.; Zhao, X. L.; Chu, K. Atomically Fe-doped MoS_{2-x} with Fe–Mo dual sites for efficient electrocatalytic NO reduction to NH_3. *Appl. Catal. B: Environ.* **2023**, *324*, 122241.

[58] Wang, D. D.; Fan, G. L.; Pei, Z. H.; Luan, D. Y.; Gu, X. J.; Lou, X. W. D. Efficient Cu–Co dual-sites in cobalt oxide nanoboxes for electrocatalytic reduction of low-concentration NO to NH_3. *Adv. Mater.* **2025**, *37*, 2504497.

[59] Wang, D. D.; Zhu, X. R.; Tu, X. J.; Zhang, X. R.; Chen, C.; Wei, X. X.; Li, Y. F.; Wang, S. Y. Oxygen-bridged copper-iron atomic pair as dual-metal active sites for boosting electrocatalytic NO reduction. *Adv. Mater.* **2023**, *35*, 2304646.

[60] Chen, L.; Li, Q.; Li, B. J.; Sun, W. T.; Ma, J. J.; Wang, W. T. Recent progress in electrocatalytic reduction of nitric oxide to ammonia. *Mol. Catal.* **2023**, *549*, 113531.

[61] Zhang, L. C.; Liang, J.; Wang, Y. Y.; Mou, T.; Lin, Y. T.; Yue, L. C.; Li, T. S.; Liu, Q.; Luo, Y. L.; Li, N. et al. High-performance electrochemical NO reduction into NH_3 by MoS_2 nanosheet. *Angew. Chem., Int. Ed.* **2021**, *60*, 25263–25268.

[62] Xiao, L.; Mou, S. Y.; Dai, W. D.; Yang, W. P.; Cheng, Q.; Liu, S.

Y.; Dong, F. Identification of Cu (111) as superior active sites for electrocatalytic NO reduction to NH_3 with high single-pass conversion efficiency. *Angew. Chem., Int. Ed.* **2024**, *63*, e202319135.

[63] Liang, J.; Liu, P. Y.; Li, Q. Y.; Li, T. S.; Yue, L. C.; Luo, Y. S.; Liu, Q.; Li, N.; Tang, B.; Alshehri, A. A. et al. Amorphous boron carbide on titanium dioxide nanobelt arrays for high-efficiency electrocatalytic NO reduction to NH_3. *Angew. Chem., Int. Ed.* **2022**, *61*, e202202087.

[64] Wang, H. S.; Abruña, H. D. Coupled differential electrochemical mass spectrometry and surface-enhanced infrared absorption spectroscopic studies unravel the mechanism of nitric oxide electroreduction on platinum. *J. Am. Chem. Soc.* **2025**, *147*, 9352–9364.

[65] Wan, H.; Bagger, A.; Rossmeisl, J. Electrochemical nitric oxide reduction on metal surfaces. *Angew. Chem., Int. Ed.* **2021**, *60*, 21966–21972.

[66] Kim, D. H.; Ringe, S.; Kim, H.; Kim, S.; Kim, B.; Bae, G.; Oh, H. S.; Jaouen, F.; Kim, W.; Kim, H. et al. Selective electrochemical reduction of nitric oxide to hydroxylamine by atomically dispersed iron catalyst. *Nat. Commun.* **2021**, *12*, 1856.

[67] Liao, P. S.; Kang, J. W.; Xiang, R.; Wang, S. H.; Li, G. Q. Electrocatalytic systems for NO_x valorization in organonitrogen synthesis. *Angew. Chem., Int. Ed.* **2024**, *63*, e202311752.

[68] Chen, J. J.; Liu, Y. Z.; Liu, Q. Y.; Li, X. N.; He, S. G. Single Ti^{3+} Ion catalyzes NO reduction on stoichiometric titanium oxide cluster anions $(TiO_2)_n^-$ (n = 1–11). *ACS Catal.* **2022**, *12*, 8768–8775.

[69] Wang, Z. L.; Duan, H. Y.; Qu, W. Q.; Han, D. L.; Li, X. C.; Zhu, L.; Jiang, X.; Cheng, D. H.; Shen, Y. J.; Xie, M. et al. Sulfur mediated interfacial proton-directed transfer boosts electrocatalytic nitric oxide reduction to ammonia over dual-site catalysts. *Angew. Chem., Int. Ed.* **2025**, *64*, e202511398.

[70] Liang, J.; Zhou, Q.; Mou, T.; Chen, H. Y.; Yue, L. C.; Luo, Y. S.; Liu, Q.; Hamdy, M. S.; Alshehri, A. A.; Gong, F. et al. FeP nanorod array: A high-efficiency catalyst for electroreduction of NO to NH_3 under ambient conditions. *Nano Res.* **2022**, *15*, 4008–4013.

[71] Rao Nulakani, N. V.; Kumar Choutipalli, V. S.; Shuford, K. L.; Ali, M. A. Boronated aromatic ring-fused structure: An efficient electrocatalyst for sustainable ammonia synthesis from nitric oxide pollutant. *Fuel* **2026**, *404*, 136336.

[72] Zhou, J.; Han, S. H.; Yang, R.; Li, T. L.; Li, W. B.; Wang, Y. T.; Yu, Y. F.; Zhang, B. Linear adsorption enables NO selective electroreduction to hydroxylamine on single co sites. *Angew. Chem., Int. Ed.* **2023**, *62*, e202305184.

[73] Tan, Y.; Fu, J. W.; Luo, T.; Liu, K.; Liu, M. Theoretical insights into the selectivity of single-atom Fe–N–C catalysts for electrochemical NO_x reduction. *J. Am. Chem. Soc.* **2025**, *147*, 4937–4944.

[74] Wu, Y. M.; Liu, X. Y.; Yang, R.; Cheng, C. Q.; Song, Z. Y.; Zhang, B. Ampere-level electrosynthesis of a nylon-6 precursor by local NO coverage tuning. *Nat. Synth.* **2025**, *4*, 1504–1512.

[75] Ko, B. H.; Hasa, B.; Shin, H.; Zhao, Y. R.; Jiao, F. Electrochemical reduction of gaseous nitrogen oxides on transition metals at ambient conditions. *J. Am. Chem. Soc.* **2022**, *144*, 1258–1266.

[76] Long, J.; Guo, C. X.; Fu, X. Y.; Jing, H. J.; Qin, G. Q.; Li, H.; Xiao, J. P. Unveiling potential dependence in NO electroreduction to ammonia. *J. Phys. Chem. Lett.* **2021**, *12*, 6988–6995.

[77] Qian, S. J.; Cao, H.; Wang, Y. G.; Li, J. Controlling the selectivity of electrocatalytic NO reduction through pH and potential regulation on single-atom catalysts. *J. Am. Chem. Soc.* **2024**, *146*, 12530–12537.

[78] Wang, S. W.; Xia, J. K.; Yang, X. H.; Xie, Q.; Zhuang, Z. C.; Feng, H. J.; Xiang, H.; Chen, Z. L.; Li, H.; Zhang, L. et al. Two-dimensional materials for NO_x reduction to ammonia: From electrocatalyst to system. *Coord. Chem. Rev.* **2025**, *535*, 216610.

[79] Yuan, R.; Jiao, H. D.; Zhu, H. M.; Fang, D. N.; Jiao, S. Q. *In situ* characterization techniques and methodologies for high-temperature electrochemistry. *Chem* **2023**, *9*, 2481–2508.

[80] Yu, Q.; Sun, S. H.; Puente-Santiago, A. R.; Wu, C. L.; Xiong, X. Q.; Jin, Y. X.; Weng, B. Zinc mediated electronic structure of CoP toward photocatalytic H_2 evolution. *Appl. Catal. B: Environ. Energy* **2025**, *367*, 125098.

[81] Sheng, J. P.; He, Y.; Zhong, F. Y.; Du, C. Y.; Liang, G. J.; Ma, X. D.; Sun, Y. J.; Dong, F. Turn waste into treasure: Gas–solid photoreduction of NO in flow for separation-free ammonia synthesis. *Environ. Sci. Technol.* **2025**, *59*, 19002–19011.

[82] Yang, W. Q.; Liu, H.; Chang, X. X.; Zhang, Y. L.; Cai, Y. F.; Li, Y. F.; Cui, Y.; Xu, B. J.; Yu, L.; Cui, X. J. et al. Electrosynthesis of NH_3 from NO with Ampere-level current density in a pressurized electrolyzer. *Nat. Commun.* **2025**, *16*, 1257.

[83] He, Y.; Sheng, J. P.; Ren, Q.; Sun, Y. J.; Hao, W. C.; Dong, F. *Operando* identification of dynamic photoexcited oxygen vacancies as true catalytic active sites. *ACS Catal.* **2023**, *13*, 191–203.

[84] Shen, S. J.; Chen, R. M.; Li, X.; Wang, J. L.; Yu, S. S.; Li, J. Y.; Dong, F. Regulating the selectivity of nitrate photoreduction for purification or ammonia production by cooperating oxidative half-reactions. *Environ. Sci. Technol.* **2024**, *58*, 7653–7661.

[85] Clayborne, A.; Chun, H. J.; Rankin, R. B.; Greeley, J. Elucidation of pathways for NO electroreduction on Pt (111) from first principles. *Angew. Chem.* **2015**, *127*, 8373–8376.

[86] Liu, J. Y.; Wang, S. A.; Tian, Y. Y.; Guo, H. Q.; Chen, X.; Lei, W. W.; Yu, Y. F.; Wang, C. H. Screening of silver-based single-atom alloy catalysts for NO electroreduction to NH_3 by DFT calculations and machine learning. *Angew. Chem., Int. Ed.* **2025**, *64*, e202414314.

[87] Abild-Pedersen, F.; Greeley, J.; Studt, F.; Rossmeisl, J.; Munter, T. R.; Moses, P. G.; Skúlason, E.; Bligaard, T.; Nørskov, J. K. Scaling properties of adsorption energies for hydrogen-containing molecules on transition-metal surfaces. *Phys. Rev. Lett.* **2007**, *99*, 016105.

[88] Yin, H.; Gong, M. H.; Lyu, P. B.; Wang, R.; Sun, L. Z. Theoretical insights into the selective electrocatalytic reduction of NO to NH_3 on a two-dimensional Cu-Benzylthiol metal–organic framework nanostructure. *ACS Appl. Nano Mater.* **2024**, *7*, 5180–5191.

[89] Deshpande, S.; Greeley, J. First-principles analysis of coverage, ensemble, and solvation effects on selectivity trends in NO electroreduction on Pt_3Sn alloys. *ACS Catal.* **2020**, *10*, 9320–9327.

[90] Yang, L.; Fan, J. K.; Xiao, B. B.; Zhu, W. H. Unveiling "Sabatier principle" for electrocatalytic nitric oxide reduction on single cluster catalysts: A DFT and machine learning guideline. *Chem. Eng. J.* **2023**, *468*, 143823.

[91] Li, J. Y.; Wang, J. L.; Shen, S. J.; Chen, R. M.; Liu, M.; Dong, F. Beyond purification: Highly efficient and selective conversion of NO into ammonia by coupling continuous absorption and photoreduction under ambient conditions. *Environ. Sci. Technol.* **2023**, *57*, 5445–5452.

[92] Cheon, S.; Kim, W. J.; Kim, D. Y.; Kwon, Y.; Han, J. I. Electro-synthesis of ammonia from dilute nitric oxide on a gas diffusion electrode. *ACS Energy Lett.* **2022**, *7*, 958–965.

[93] Qin, Y.; Gao, J. Y.; Huang, B. Nitric oxide-to-ammonia synthesis with nearly 100% yield by ambient-pressure thermocatalysis under mild temperature. *J. Am. Chem. Soc.* **2025**, *147*, 29673–29678.

[94] Shao, J. Q.; Jing, H. J.; Wei, P. F.; Fu, X. Y.; Pang, L.; Song, Y. P.; Ye, K.; Li, M. R.; Jiang, L. Z.; Ma, J. Y. et al. Electrochemical synthesis of ammonia from nitric oxide using a copper-tin alloy catalyst. *Nat. Energy* **2023**, *8*, 1273–1283.

[95] Meng, J. Y.; Cheng, C. Q.; Wang, Y. T.; Yu, Y. F.; Zhang, B. Carbon support enhanced mass transfer and metal–support interaction promoted activation for low-concentrated nitric oxide electroreduction to ammonia. *J. Am. Chem. Soc.* **2024**, *146*, 10044–10051.

[96] Guo, X. X.; Wu, T. W.; Li, H. F.; Zhang, Y. N.; Ma, C.; Li, H. M.; Chai, L. Y.; Zhao, H. T.; Liu, M. Electrosynthesis of NH_3 from low-concentration NO on cascade dual-site catalysts in neutral media. *Nat. Commun.* **2025**, *16*, 8481.

[97] Wu, Z.; Liu, Y. J.; Wang, D. D.; Zhang, Y. Q.; Gu, K. Z.; He, Z. J.; Liu, L. M.; Liu, H. W.; Fan, J. C.; Chen, C. et al. Cu@Co with dilatation strain for high-performance electrocatalytic reduction of low-concentration nitric oxide. *Adv. Mater.* **2024**, *36*, 2309470.

[98] Chen, H.; Gao, Y. X.; Du, J. X.; Hao, R. L.; Wu, X. H.; Wang, L. D.; Wu, Z. B. Bridging cobalt single atom satellite and nanoparticle synergies for efficient low-concentration NO electroreduction to ammonia. *ACS Nano.* **2026**, *20*, 2323–2336.

[99] Chen, L.; Meng, L.; Shi, D. L.; Wang, Y. C.; Zhang, Y. L.; Guo, J. T.; Fu, Q. Q.; Jia, Y. X.; Huang, Y. J. Nanocurvature-steered interfacial hydrogen shuttle for bosting electrocatalytic low-concentration NO reduction to ammonia. *Adv. Funct. Mater.*, in press, DOI: 10.1002/adfm.202527175.

[100] Cui, D.; Li, Y. Q.; Pan, K. K.; Liu, J. B.; Wang, Q.; Liu, M. M.; Cao, P.; Dan, J. M.; Dai, B.; Yu, F. NO hydrogenation to NH_3 over $FeCu/TiO_2$ catalyst with improved activity. *Front. Chem. Sci. Eng.* **2023**, *17*, 1973–1985.

[101] Chen, R. M.; Li, J. Y.; Wang, J. L.; Yang, W. P.; Shen, S. J.; Dong, F. Continuous NO upcycling into ammonia promoted by SO_2 in flue gas: Poison can be a gift. *Environ. Sci. Technol.* **2023**, *57*, 12127–12134.

[102] Li, Z.; Xiao, J. W.; Gao, Y. S.; Gui, R. R.; Wang, Q. Design of bifunctional Cu-SSZ-13@$Mn_2Cu_1Al_1O_x$ core–shell catalyst with superior activity for the simultaneous removal of VOCs and NO_x. *Environ. Sci. Technol.* **2023**, *57*, 20326–20338.

[103] Liu, X. Y.; Wang, P. L.; Shen, Y. J.; Zheng, L. R.; Han, L. P.; Deng, J.; Zhang, J. P.; Wang, A. Y.; Ren, W.; Gao, F. et al. Boosting SO_2-resistant NO_x reduction by modulating electronic interaction of short-range Fe–O coordination over Fe_2O_3/TiO_2 catalysts. *Environ. Sci. Technol.* **2022**, *56*, 11646–11656.

[104] Liu, Y. X.; Wang, Q.; Pan, J. F. Novel process of simultaneous removal of nitric oxide and sulfur dioxide using a vacuum ultraviolet (VUV)-activated $O_2/H_2O/H_2O_2$ system in a wet VUV-spraying reactor. *Environ. Sci. Technol.* **2016**, *50*, 12966–12975.

[105] Li, P.; Liu, Y.; Xie, L. Y. Q.; Wang, G. T.; Lu, X. Z.; Li, J.; Wu, X. H.; Jiang, Y. J.; Zhu, W. L. Mechanistic insights into the CO_2-assisted NO electrochemical deoxygenation and hydrogenation. *Angew. Chem., Int. Ed.* **2025**, *64*, e202504499.